Desalination and Water Treatment
www.deswater.com
doi: 10.1080/19443994.2015.1104726

57 (2016) 19820–19833
September

Taylor & Francis
Taylor & Francis Group

Poly (methyl methacrylate)-grafted alginate/Fe_3O_4 nanocomposite: synthesis and its application for the removal of heavy metal ions

Alok Mittal[a,*], Rais Ahmad[b], Imran Hasan[b]

[a]*Department of Chemistry, Maulana Azad National Institute of Technology, Bhopal 462003, India, Tel. +91 9425025427; Fax: +91 755 2670562; email: aljymittal@yahoo.co.in*
[b]*Environmental Research Laboratory, Department of Applied Chemistry, Aligarh Muslim University, Aligarh 202002, India, Tel. +91 0571 2700920 23 ext. 3000; Fax: +91 0571 2400528; emails: rais45@rediffmal.com (R. Ahmad), imranhasan98@gmail.com (I. Hasan)*

Received 1 September 2015; Accepted 2 October 2015

ABSTRACT

A novel adsorbent poly (methyl methacrylate)-grafted alginate/Fe_3O_4 nanocomposite was synthesized by oxidative-free radical-graft copolymerization reaction. The nanocomposite was characterized using FT-IR, X-ray diffraction, SEM, TEM, TGA and DSC techniques. The potential of nanocomposite material was explored towards the adsorption of Pb(II) and Cu(II) from aqueous media under varying operating conditions such as pH, concentration of metal ions, contact time, adsorbent dose and temperature. The optimum pH recorded for metal ions adsorption was 5. The experimental data were tested using Langmuir, Freundlich, Sips and Temkin models, and the data were best followed by Freundlich model at 50°C. The maximum sorption capacity was found to be 62.5 mg g^{-1} for Pb(II) and 35.71 mg g^{-1} for Cu(II), respectively. The concentration and temperature dependent rate constants were evaluated using various kinetic models, and the data were best followed by pseudo-second-order kinetic model. The thermodynamic parameters such as enthalpy, entropy and free energy of activation were calculated to explain the nature of adsorption process.

Keywords: Bio-polymer; Sips; Heavy metals; SEM; Fe_3O_4; Adsorption

1. Introduction

The impact of heavy metals to the environment and the animals on the earth is a very serious issue due to rapid industrialization and human activity [1,2]. Pb(II) is one of the most toxic heavy metal which constitutes major environmental health disorders among the heavy metals [3–5]. The Pb(II) exposure may cause damage to organs including brain, kidneys, liver, heart and causes oedema to the immune system [6,7]. Although copper is an essential element for human beings in trace amount due to the fact that human body can regulate the trace level haemostatically, it can also be toxic when ingested beyond the permissible level [8,9]. Copper toxicity causes skin irritation, stomach disorder, kidney damage, anaemia, hepatic damage and gastrointestinal irritation in human beings [10].

Due to the above serious problems caused by heavy metals, there is a great interest for the

*Corresponding author.

removal of the heavy metal ions from wastewaters considering their toxic nature towards human health and ecosystems [11,12]. There are many processes that have been developed to reduce heavy metal pollution such as membrane filtration, ion exchange, solvent extraction, chemical precipitation, electrode deposition and adsorption [13–16]. Among the techniques used for the heavy metal removal, adsorption is most auspicious and widely used methods due to its effectiveness in metal removal to low level, abundance, economic and ease of handling [17,18].

Super-adsorbent composites based on polysaccharide and metal oxide nanoparticle have recently gained attention and may be used as alternative for adsorption studies as compared to synthetic polymer-based nanocomposite [19,20]. The small addition of nanoparticle enhances their thermal and mechanical properties significantly because of the large contact area between polymer and nanoparticle on a nanoscale [21].

Sodium alginate (SA), a linear polysaccharide of (1, 4) linked α-L-guluronate and β-D-mannuronate, has attracted more attention as an adsorbent for the removal of heavy metals [22,23]. It was preferred over other adsorbent materials because of its immunogenicity, hydrophilicity, biodegradability, abundance in nature and ability to form gels with a variety of cross-linking agents [24,25].

Magnetic nanoparticles (MNPs) are one of the most interesting and technologically important materials of physical and chemical properties with many promising applications [26]. Since their introduction, MNPs-based solid phase extraction (MNPs–SPE) has been shown to be an efficient technique to reduce trace amounts of organic and inorganic analytes from complex media [27]. Polymer-modified magnetic materials, resulting in large surface area and large adsorption sites, have been developed to remove the diverse pollutants from water samples [28].

In this study, a novel adsorbent PMMA-gft-Alg/Fe_3O_4 has been synthesized by oxidative-free radical-graft co-polymerization reaction and has been evaluated for the removal of Pb(II) and Cu(II) from their aqueous solutions. Batch technique was performed to optimize various parameters such as contact time, pH, dosage, temperature and initial metal ion concentration. The adsorbent was characterized by FT-IR, X-ray diffraction (XRD), SEM, TEM, TGA and DSC techniques. The isothermal, kinetic and thermodynamic behaviour of adsorbent towards Pb(II) and Cu(II) was also investigated.

2. Experimental

2.1. Reagents

Methyl methacrylate (99%) was purchased from Loba Chemie India, SA was purchase from Sigma-Aldrich (India), $FeCl_3{\cdot}6H_2O$, $FeCl_2{\cdot}4H_2O$, nitrate salts of Pb(II) and Cu(II) were purchase from Merck India. Liquor ammonia (25%) was purchased from Fischer Scientific India. The stock solutions of Pb(II) and Cu (II) were prepared by dissolving appropriate amount of corresponding nitrate salts of the metal ions in double distilled water.

2.2. Synthesis of Fe_3O_4 nanoparticles

Fe_3O_4 nanoparticles were synthesized by co-precipitation from a mixture of Fe(II) and Fe(III) salts reported elsewhere [29]. The detailed preparation procedure is as follows: $FeCl_3{\cdot}6H_2O$ (10.0 g) and $FeCl_2{\cdot}4H_2O$ (5.0 g) were weighed and dissolved in deionized water (300 ml) and stirred for 2 h on magnetic stirrer at 80˚C. $NH_3{\cdot}H_2O$ (20 ml of 8 mol L^{-1}) was then slowly added into the mixture solution of $FeCl_3$ and $FeCl_2$ with vigorous stirring under N_2 gas to prevent oxidation until the pH reached 10. After precipitation, the Fe_3O_4 nanoparticles were repeatedly washed using deionized water and ultrasonically treated to prevent aggregation until the pH reached 7. Finally, Fe_3O_4 nanoparticles were sterilized at 100˚C for 1 h.

2.3. Synthesis of PMMA-gft-Alg/Fe_3O_4

The synthesis was done using already reported method with slight modification [30]. First 1 g of above prepared Fe_3O_4 nanoparticles was dispersed in 100 ml of deionized water using sonicator for 30 min. Then, 2 g of alginate was dissolved in 200 ml of deionized water in a three-neck round-bottomed flask by stirring at 40˚C. To this solution, 20 ml of MMA monomer was added with 0.75 g N,N´-methylene bisacrylamide and stirred for 1 h at 60˚C. Now, the above colloidal nanoparticle dispersion of Fe_3O_4 MNPs was added to the above solution with 20 ml of 3% KPS solution as initiator, and the reaction was continued for 6 h at 60˚C in N_2 atmosphere. The obtained nanocomposite emulsion was poured in excess amount of methyl alcohol to stop the polymerization reaction and the product was then washed with distilled water until it is free from homo-polymer and dried at 60˚C for 2 h in a hot air oven, ground and then sieved to obtain 80–230 mesh sizes.

2.4. Characterization

The FTIR spectra of the adsorbent materials were recorded with a Perkin-Elmer 1800 model IR spectrophotometer operating at frequency range from 400 to 4,000 cm^{-1} using KBr pallets. XRD patterns of the samples were obtained using Siemens D 5005 X-ray unit Cu Kα (λ = 1:5406 Å) radiation, generated at a voltage of 40 kV and a current of 40 mA was used as the X-ray source. Scanning electron microscopy and electron diffraction scattering (SEM) analysis were done using JEOL GSM 6510LV scanning electron microscope. The particle size and structure of the synthesized nanocomposite were observed using JEOL JEM 2100 transmission electron microscope (TEM). Differential scanning calorimetry (DSC) thermograms were recorded with a Perkin-Elmer Pyris 6 under N_2 at a heating rate of 10°C min^{-1} to measure glass transition temperature (T_g). Thermo-gravimetric analysis was performed with DuPont Instruments (TGA 951) analyser at 10°C min^{-1} heating rate under nitrogen atmosphere in the temperature range of 30–800°C to determine dynamic weight loss. The concentration of metal ions in the solution was measured by Atomic Absorption Spectrophotometer (AAS) model GBC-902. Elico Li 120 pH metre was used to adjust the pH of the solutions.

2.5. Batch adsorption studies

The adsorption of Pb(II) and Cu(II) was investigated in batch equilibrium experiments. The stock solutions of metal ions (1,000 mg L^{-1}) were prepared using standard solutions in distilled water. The experiments were performed at pH 5 in 100 mL conical flasks containing metal ion solutions 50 mg L^{-1} and the adsorbents (0.05 g), shaken for 24 h at 120 rpm in a shaker at 50°C. Also the dosage of adsorbents, time, pH and metal ion concentration was varied to study the effect of these parameters on adsorption. To study the effect of time, the adsorption time was set from 5 to 360 min, and experiments were carried out by shaking 0.05 g of adsorbents with 50 mg L^{-1} of metal ion solution at pH 5. The amount of adsorbents was varied from 10 to 100 mg with 50 mg L^{-1} of metal ion solution and the experiment was carried out for 180 min at pH 5. The adsorption studies were carried out at different pH values ranging from 1 to 6, shaking 0.05 g of adsorbents with 50 mg L^{-1} of metal ion solution. After the desired incubation period for each batch, the aqueous phase was separated from the materials, and the concentration of metal ions was measured using AAS. The amount of metal adsorbed was calculated using following equation:

$$q_e = \frac{(c_o - c_e)V}{W} \quad (1)$$

where q_e is the amount of metal ion adsorbed per unit weight of the adsorbent (mg g^{-1}); c_o and c_e are the concentrations of the metal ion in the initial solution (mg L^{-1}) and after adsorption, respectively; V is the volume of the adsorption medium (L); W is the amount of the adsorbent (g). The value of q_{max} was calculated from q_e using the Langmuir and Freundlich linear isotherms and the corresponding values were obtained using a linear method.

2.6. Desorption

The heavy metal ions adsorbed on the hydrogel composite were desorbed by HCl solution (0.1 M, 20 mL) for 3 h at 30°C. After filtration, the concentrations of the metal ions in the aqueous phase were determined by AAS. Desorption (%) was calculated on the basis of Eq. (2):

$$\%\,\text{des} = \frac{M_{des}}{M_{ads}} \times 100 \quad (2)$$

where M_{ads} is the amount of metal ion adsorbed onto nanocomposite (mg g^{-1}) and M_{des} is the amount of metal ion desorbed (mg g^{-1}).

3. Results and discussion

3.1. Characterization

Fig. 1 shows the FTIR spectra of pure Fe_3O_4 MNPs, SA, PMMA and PMMA-gft-Alg/Fe_3O_4 nanocomposite. The FTIR spectrum of Fe_3O_4 MNPs shows high-intensity band at 583 cm^{-1} corresponds to the Fe–O stretching vibration from the magnetite [31], and bands at 1,631 and 3,393 cm^{-1} can be assigned to the O–H stretching modes and bending vibration of Fe_3O_4, respectively. FTIR spectrum of alginate exhibited absorption bands at 3,450 cm^{-1} (OH stretching), 2,920 cm^{-1} (CH_2 stretching), 1,622 cm^{-1} (COO– asymmetric stretching) and 1,426 cm^{-1} (COO– symmetric stretching) [32]. It can be seen from the FTIR spectrum of PMMA that there is a distinct absorption band from 1,150 to 1,246 cm^{-1}, which can be attributed to the C–O–C stretching vibration. The band at 978 cm^{-1} is the characteristic absorption vibration of PMMA. The band at 1,730 cm^{-1} shows the presence of the acrylate carboxyl group. The band at 1,438 cm^{-1} can be attributed to the bending vibration of the C–H bonds of the $–CH_3$ group. The two bands at 2,996 and 2,950 cm^{-1}

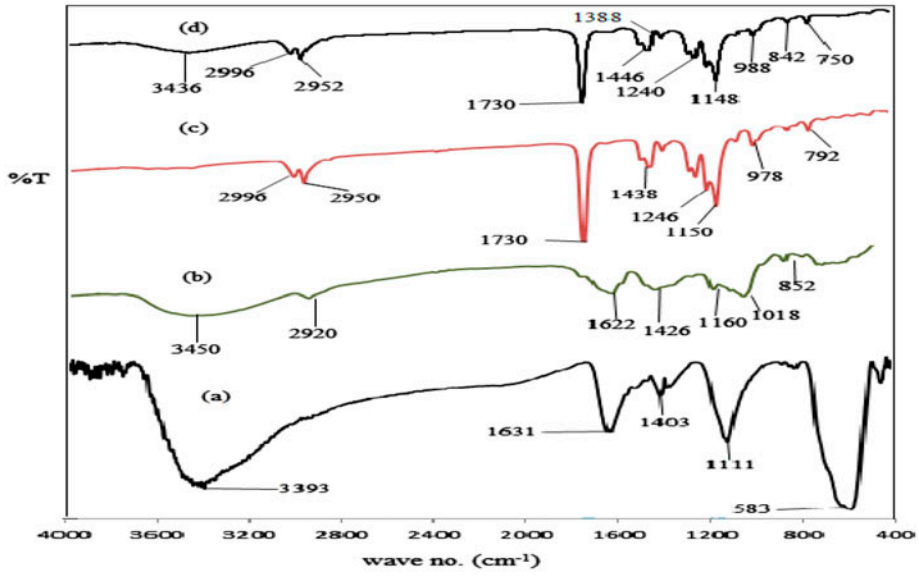

Fig. 1. FTIR Spectra of (a) Fe_3O_4, (b) alginate, (c) PMMA and (d) PMMA-gft-Alg/Fe_3O_4.

can be assigned to the C–H bond stretching vibrations of the $–CH_3$ and $–CH_2–$ groups, respectively [33]. In the spectrum of PMMA-gft-Alg/Fe_3O_4 nanocomposite shows all the bands related to PMMA. The broad band at 3,446 cm^{-1} is due to –OH stretching from both Fe_3O_4 and alginate which confirms the formation of nanocomposite material.

The XRD patterns of Fe_3O_4 nanoparticles, SA, PMMA and PMMA-gft-Alg/Fe_3O_4 nanocomposite are shown in Fig. 2. In the XRD pattern of uncoated Fe_3O_4 MNPs, diffraction peaks were observed at 30.4370, 31.8948, 35.8414, 43.4590, 53.8936, 57.3527, 62.9424 and 74.4688 at 2θ scale. Incorporation and uniform distribution of Fe_3O_4 MNPs in PMMA-gft-Alg polymer matrix was confirmed by the presence of all the XRD peaks mentioned above in the XRD pattern of PMMA-gft-Alg/Fe_3O_4 nanocomposite with a little bit of reduced intensity and the peaks became slightly wider because of the coating of non-magnetic and amorphous PMMA-gft-Alg polymeric matrix [34].

The TGA thermograms of PMMA-gft-Alg and PMMA-gft-Alg/Fe_3O_4 nanocomposite are shown in Fig. 3.The TG curve presented that PMMA-gft-Alg decomposed in three stages. The first stage of PMMA-gft-Alg decomposition (about 91.20˚C) is due to the loss of water and methyl methacrylate from the additive as well as residual acetone. The second stage decomposition begins at about 191.28˚C, which might be due to the radical transfer to unsaturated chain ends. The weight loss with third stage (about 389.97˚C) associated with random scission of the polymer backbone [35]. The TGA thermogram of the PMMA-gft-Alg/Fe_3O_4 composite also presented three stages of decomposition. The thermogram clearly indicated that the second and third stage of decomposition of the composite were shift to higher temperature as compared to PMMA-gft-Alg matrix. The TGA thermograms indicated that the incorporation of Fe_3O_4 MNPs enhanced the thermal degradation of PMMA-gft-Alg.

Glass transition temperatures (T_g) of these organic–inorganic hybrid materials were characterized by DSC. The thermo-scan profiles were depicted in Fig. 4 for PMMA-gft-Alg and PMMA-gft-Alg/Fe_3O_4 nanocomposite. It can be found that neat PMMA-gft-Alg has an obvious single T_g at 121.87˚C. However, synthesized PMMA-gft-Alg/Fe_3O_4 also exhibited single T_g. The hybrid material exhibited only single but tremendous wide profile of glass transition in DSC measurement. Also could be seen that the T_g of hybrid material (118.14˚C) was lower than that of PMMA-gft-Alg, which indicated that the embodiment of Fe_3O_4 MNPs promoted the polymer thermal properties by providing crystallinity to the amorphous polymer matrix, which was due to existence of the strong interactions between the Fe_3O_4 MNPs and the polymer matrix.

The fractured surface of the hybrid nanocomposite material was observed using SEM, which can give important information about the morphology of these materials. The SEM images of PMMA, alginate and PMMA-gft-Alg/Fe_3O_4 nanocomposite are shown in Fig. 5. SEM image of PMMA is granules having a spherical shape with various sizes and for alginate irregular spherical granules. However, the composite appears highly porous in nature which is very much

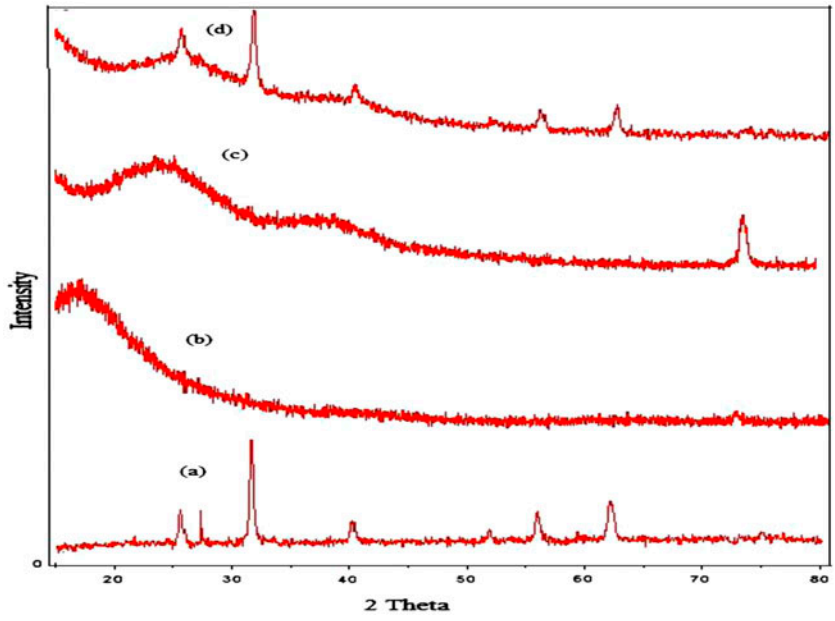

Fig. 2. XRD Spectra of (a) Fe_3O_4, (b) alginate, (c) PMMA and (d) PMMA-gft-Alg/Fe_3O_4.

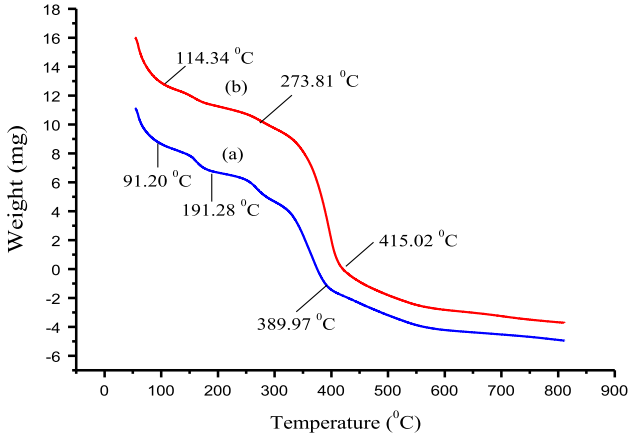

Fig. 3. TGA thermograms of (a) PMMA-gft-Alg and (b) PMMA-gft-Alg/Fe_3O_4.

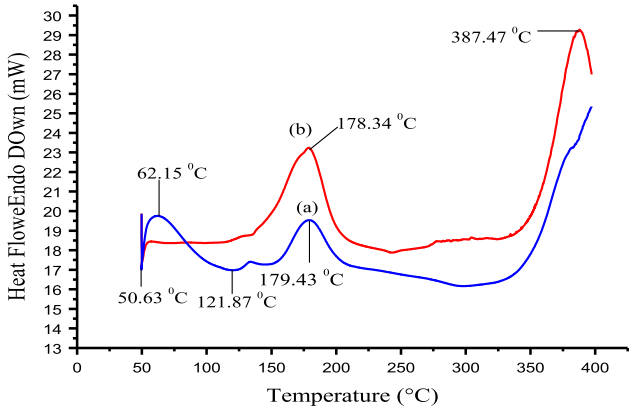

Fig. 4. DSC thermograms of (a) PMMA-gft-Alg and (b) PMMA-gft-Alg/Fe_3O_4.

different from the starting products PMMA and alginate. This change in surface morphology supported the occurrence of graft polymerization. The change in surface morphology may influence the penetration of water into the polymer network, and it may affect swelling ability of the corresponding magnetic nanocomposite [36].

The TEM image of PMMA-gft-Alg/Fe_3O_4 is shown in Fig. 6 from which it is clear that Fe_3O_4 MNPs are uniformly distributed in the polymer matrix and showing an average diameter of 132 nm. This bigger size of Fe_3O_4 MNPs is due to the coating of polymer on the nanoparticle surface.

3.2. Adsorption Studies for Pb(II) and Cu(II)

3.2.1. Effect of pH

The effect of pH plays an important role on the active sites of adsorbent as well as the heavy metal speciation during the adsorption reaction. In order to evaluate the influence of pH on the adsorption capacity of the PMMA-gft-Alg/Fe_3O_4, experiments were carried out at initial concentration of 50 mg L^{-1} and in the pH range 1.0–6.0 at 50°C. It can be seen from Fig. 7a that the adsorption capacities increase from 15.06 to 18.76 mg g^{-1} for Pb(II) and 10.05–16.78 mg g^{-1} for Cu(II) as pH values rise from 1 to 5 and then

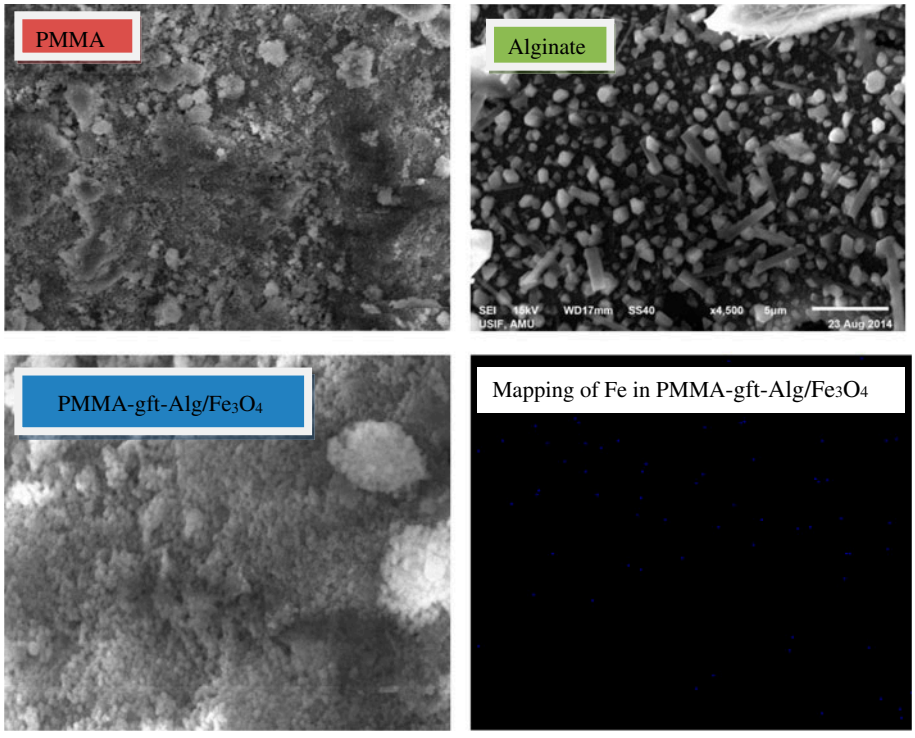

Fig. 5. SEM Images of (a) PMMA, (b) Alginate, (c) PMMA-gft-Alg/Fe_3O_4 and (d) Mapping for Fe in the PMMA-gft-Alg/Fe_3O_4.

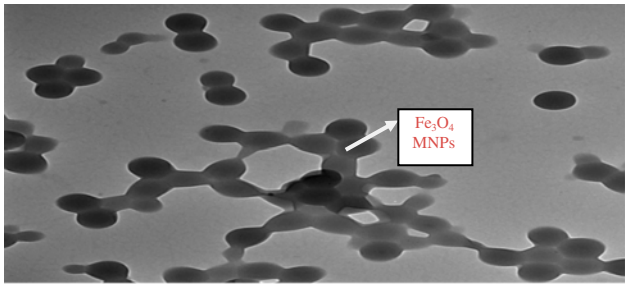

Fig. 6. TEM image of PMMA-gft-Alg/Fe_3O_4 nanocomposite showing the distribution of Fe_3O_4 nanoparticle in polymer matrix.

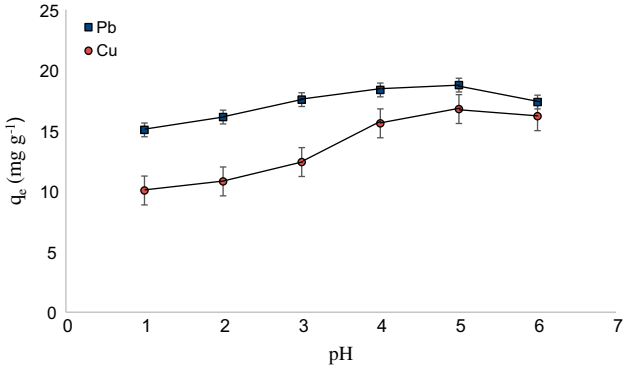

Fig. 7a. Effect of pH on PMMA-gft-Alg/Fe_3O_4 for the removal of metal ions with $c_o = 50$ mg L^{-1} and 0.05 g adsorbent dosage at 50°C.

decrease slightly with further increase of pH values. At low pH values, the adsorption capacities are low due to the large quantities of coexisting H^+ ions which can also be adsorbed onto the composite.

However, if pH values are high (over 7), poor solubility of the metal salts is observed. At initial pH < 5.0, H^+ ions competed with metal ions for the surface of the adsorbent, which would restrict the approach of metal ions due to the repulsion [37]. Hence, the metal removal was the lower amount presumably due to the enhanced competition of proton with metal ions for ligand-binding sites and complex formation. On the other hand, the adsorptive behaviour of Pb(II) and Cu(II) ions is pH dependent because the pH values also affected the charge on the adsorbent surface. At pH < 5.0, metal ions can be repelled by the surface positive charges on the adsorbent due to the protonation of oxygen groups (R-OH_2^+). The behaviour of adsorbent towards metals ions with respect to pH can be attributed by the point of zero charge study of the adsorbent. The point of

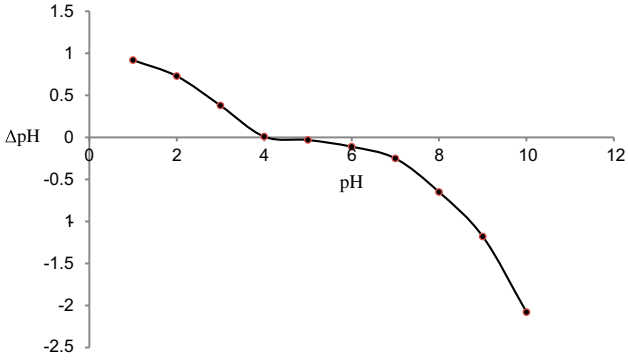

Fig. 7b. Point of zero charge for the PMMA-gft-Alg/Fe_3O_4 using Standard 0.1 M KCl Solution.

zero charge was found at 4 and is shown in Fig. 7b. The adsorption of metal ions increased as the initial pH of the system increased, metal ions are attached on the surface of nanocomposite by replacing H^+ ions of the carboxylic and phenolic ions until a maximum yield is reached. The condition of initial pH > 5.0, recorded a decrease in adsorption, which may be attributed to precipitation of the metal ions as hydroxides. For this reason, the optimal pH value was selected to be 5.0 for both Pb(II) and Cu(II) as it shows maximum adsorption capacity at pH 5.0.

3.2.2. Effect of initial metal ion concentration

The results obtained for the adsorption upon varying the initial heavy metal ions concentrations (20–100 mg L^{-1}) at 50°C is illustrated in Fig. 8. The figure itself indicates that as the metal ion concentration increases from 20 to 100 mg L^{-1}, the adsorption capacity also increases from 7.44 to 34.56 mg g^{-1} for Pb(II) and 7.12 to 25.35 mg g^{-1} for Cu(II). The increase in the loading capacity of adsorbent with increasing heavy metal concentrations is due to the interaction between metal ions and adsorbent which provides the vital driving force to defeat the resistances to the mass transfer of metal ions between the aqueous solution and the adsorbent [38]. As the initial concentration increases, the adsorption capacity of the adsorbent increases sharply in the beginning and the adsorption of the adsorbent tends to increase with increase in heavy metal ion concentration due to an increase in electrostatic interactions, which involves active sites of progressively lower affinity for the heavy metal ions up to saturation point.

3.2.3. Effect of contact time and temperature

The time profiles of metal ions sorption between 5 and 360 min by PMMA-gft-Alg/Fe_3O_4 nanocomposite at 50°C are presented in Fig. 9, respectively. The amount of metal ions adsorbed did not increase with contact time until the plateau, implying equilibrium was reached. The amount of metal ions adsorbed rapidly in the initial stage was due to the availability of binding sites of the adsorbent, but as time went by, the sorption slowed down before reaching equilibrium at about 180 min. The equilibrium values of Pb(II) 19.92 mg g^{-1}, Cu(II) 16.8 mg g^{-1} could be achieved at a high level of adsorption efficiency.

To analyse the effect of temperature on adsorption of heavy metal ions, experiments were performed at 30, 40 and 50°C with 50 mg L^{-1} initial metal ion concentration in a water bath shaker incubator (120 rpm) for 180 min. It was seen that by increasing the temperature, the adsorption capacity of the adsorbent increases showing that the adsorption of Pb(II) and Cu(II) on PMMA-gft-Alg/Fe_3O_4 nanocomposite follows an endothermic process and could be elucidated

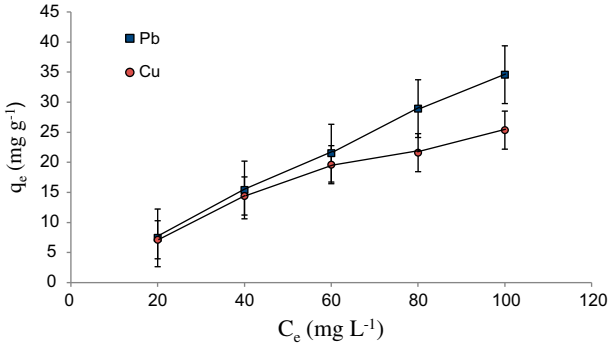

Fig. 8. Effect of initial metal ion concentration on PMMA-gft-Alg/Fe_3O_4 for the removal of metal ions with 0.05 g adsorbent dose and pH 5 at 50°C.

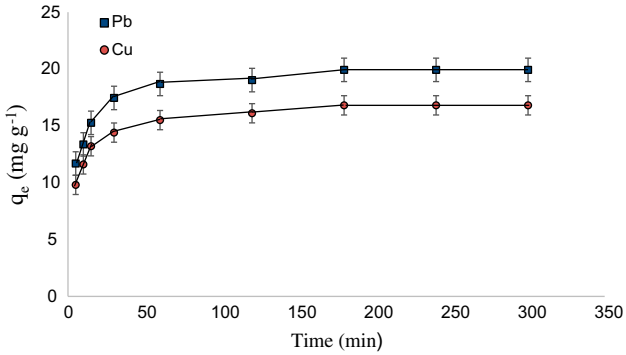

Fig. 9. Effect of time on PMMA-gft-Alg/Fe_3O_4 for the removal of metal ions at c_o = 50 mg L^{-1}, 0.05 g adsorbent dosage and pH 5 at 50°C.

by availability of more active sites of adsorbent, the enlargement and activation of the adsorbent surface at higher temperatures. This could also be due to the easy mobility of heavy metals ions from the bulk solution towards the adsorbent surface and enhanced the accessibility to the adsorbent active sites. So, 50°C was chosen as the optimum temperature for all adsorption reactions.

3.2.4. Effect of adsorbent dose

The effect of PMMA-gft-Alg/Fe_3O_4 dosage (10–100 mg) on the removal efficiencies of Pb(II) and Cu(II) was investigated and the results are listed in Fig. 10. It was found that the adsorption efficiency of the metal ions increased with increasing initial amount of adsorbent doses and the maximum capacity of 19.95 and 17.94 mg g^{-1} for Pb(II) and Cu(II) was observed, respectively.

3.3. Adsorption kinetics

Kinetics of the adsorption process is vital parameter which provides essential information on the solute uptake rate and the reaction pathways. To determine the rate-determining step during the adsorption process, the kinetic data of heavy metals onto PMMA-gft-Alg/Fe_3O_4 were simulated with the pseudo-first order and pseudo-second order, Elovich and Weber–Morris intra-particle diffusion models.

The pseudo-first-order kinetics model is based on the assumption that adsorption was controlled by diffusion steps [39] and the rate of adsorption is in direct proportion to the difference value of equilibrium adsorption capacity and the adsorption capacity at any time t. The linear equation for this model can be expressed by following equation as follows:

$$\log(q_e - q_t) = \log q_e - \frac{k_1}{2.303}t \tag{3}$$

where k_1 is the pseudo-first-order rate constant (min^{-1}), q_e is the amount of heavy metal ions adsorbed at equilibrium (mg g^{-1}), and q_t is the amount of the adsorption at any time t (mg g^{-1}). Such an equation should yield a straight line Fig. 11 with intercept equal to log q_e and slope equal to (k_1/2.303).

The linear equation for pseudo-second-order kinetics [40] is given by the following equation:

$$\frac{t}{q_t} = \frac{1}{k_2 q_e^2} + \frac{t}{q_e} \tag{4}$$

where k_2 is the pseudo-second-order rate constant (g mg^{-1} min^{-1}), q_e is the amount of heavy metal ions adsorbed at equilibrium (mg g^{-1}), and q_t is the amount of the adsorption at any time t (mg g^{-1}). The linear plot of pseudo-second-order model is given in Fig. 12 from which constant k_2 and q_e can be calculated.

If the process is a chemisorption on highly heterogeneous sorbents, the sorption kinetics could be interpreted by Elovich equation as follows:

$$q_t = \frac{1}{\beta}\ln t + \frac{1}{\beta}\ln(\alpha\beta) \tag{5}$$

where is α the initial adsorption rate (mg g^{-1} min^{-1}) and β is the adsorption constant (g mg^{-1}). q_t is the adsorption capacity at any time t in mg g^{-1}. Fig. 13 shows a plot of linearization form of Elovich model. The slopes and intercepts of plots of q_t vs. ln t were

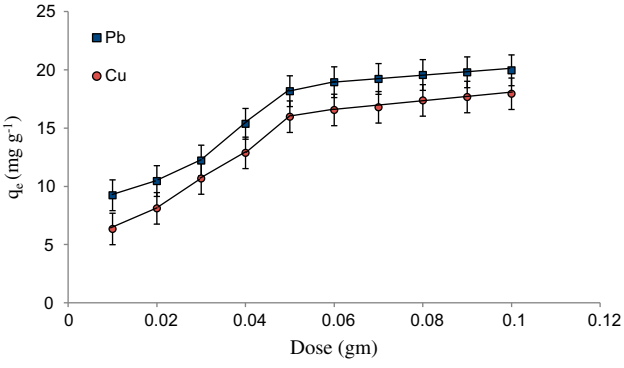

Fig. 10. Effect of adsorbent dosage for the removal of heavy metal ions on PMMA-gft-Alg/Fe_3O_4 with initial metal ion concentration 50 mg L^{-1} and pH 5 at 50°C.

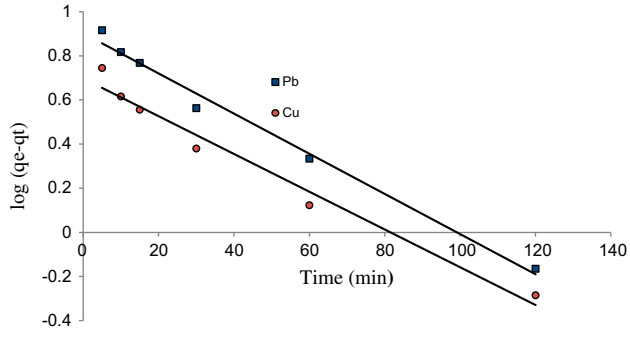

Fig. 11. Pseudo-first-order model for Pb(II) and Cu(II) ions at c_o = 50 mg L^{-1}, 0.05 g adsorbent dosage and pH 5 at 50°C.

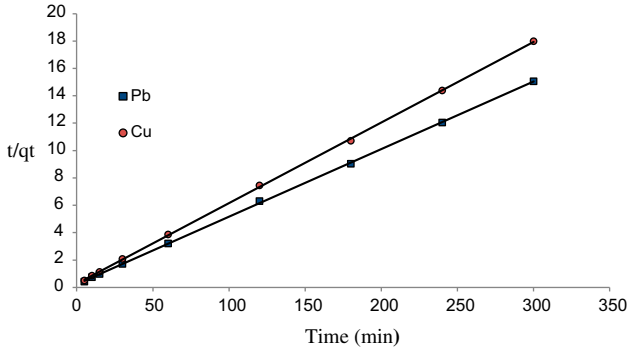

Fig. 12. Pseudo-second-order model for Pb(II) and Cu(II) ions at c_o = 50 mg L^{-1}, 0.05 g adsorbent dosage and pH 5 at 50°C.

used to determine the constant β and the initial adsorption rate α.

When absorbates transmit from solution into solid phase such as absorbents, pore and intraparticle diffusion are often rate limiting in a batch reactor system. The intraparticle diffusion was explored using the following equation suggested by Weber and Morris [41]:

$$q_t = k_{int} t^{0.5} + C \quad (6)$$

where the parameter q_t is the amount adsorbed at time t (mg g^{-1}), k_{int} is the intraparticle diffusion equation constant (mg g^{-1} $min^{-1/2}$) and t is the time. According to the Weber–Morris model, the plot of q_t, against $t^{1/2}$, should give a straight line when diffusion plays a role in the sorption rate and should cross the origin if intraparticle diffusion is the rate-determining step. The intraparticle diffusion parameters can be calculated from the slope and intercept of the linear plot given in Fig. 14.

The kinetic parameters obtained by the sorption of heavy metal ions on PMMA-gft-Alg/Fe_3O_4 nanocomposite are summarized in Table 1. It is found

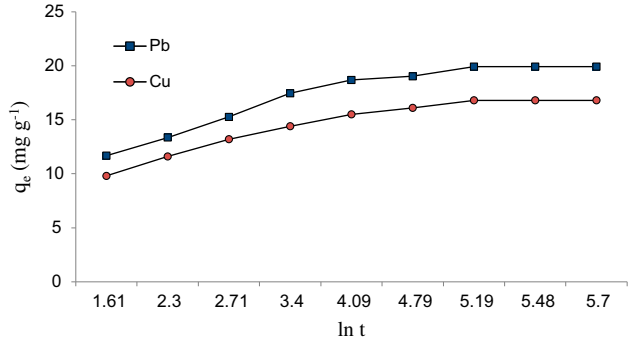

Fig. 13. Elovich model for Pb(II) and Cu(II) ions at c_o = 50 mg L^{-1}, 0.05 g adsorbent dosage and pH 5 at 50°C.

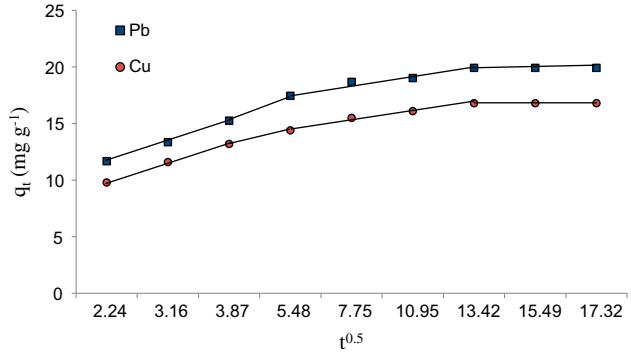

Fig. 14. Intra-particle diffusion model for Pb(II) and Cu(II) ions at c_o = 50 mg L^{-1}, 0.05 g adsorbent dosage and pH 5 at 50°C.

that the correlation coefficients R^2 for the pseudo-second-order kinetic model are 0.9999 for both Pb(II) and Cu(II) ions, respectively, that is higher than the correlation coefficient obtained for other models. Also the q_{cal} obtained through this model for Pb(II) 20.41 and 17.24 mg g^{-1} for Cu(II) much closer to q_{exp} of Pb (II) 19.92 and 16.8 mg g^{-1} for Cu(II). The pseudo-second-order kinetic model assumes that the rate-limiting step may be chemical adsorption, and the adsorption behaviour of PMMA-gft-Alg/Fe_3O_4 may involve valence forces through sharing of electrons between transition metal cations and the PMMA-gft-Alg/Fe_3O_4. The values of α calculated by Elovich model are 212.87 for Pb(II) and 213.73 for Cu(II). While the values of β are 0.49 for Pb(II) and 0.63 for Cu(II). The values of intraparticle diffusion constant (k_{int}) obtained by intraparticle diffusion model are 0.48 for Pb(II) and 0.40 for Cu(II), respectively.

Because of the fact that diffusion and adsorption are often experimentally inseparable, the uptake of metal ions onto nanocomposite may be a complicate process including diffusion, coordinating bond formation or chemical reaction simultaneously. However, from the results obtained, it can be observed that good fits to the experimental data are obtained with pseudo-second-order model for both metals.

3.4. Adsorption isotherms

The adsorption isotherms of PMMA-gft-Alg/Fe_3O_4 for Pb(II) and Cu(II) were investigated at 50°C, and the data were analysed by Langmuir and Freundlich, Sips and Temkin equations, respectively.

The Langmuir, Freundlich, Sips and Temkin isotherms equations were expressed by Eqs. (7), (8), (9) and (10) which were used for modelling of these adsorption isotherms [42–45]:

Table 1
Kinetic parameters of Pb(II) and Cu(II) ions at 50°C

Metal ions	Pseudo-first			Pseudo-second			Elovich model			Intraparticle		
	$q_{e,cal}$	k_1	R^2	$q_{e,cal}$	k_2	R^2	α	β	R^2	K_{int}	C	R^2
Pb(II) q_{exp} = 19.92 mg g^{-1}	7.99	0.02	0.98	20.41	0.01	0.99	212.87	0.49	0.93	0.48	12.97	0.77
Cu(II) q_{exp} = 16.8 mg g^{-1}	4.98	0.02	0.98	17.24	0.01	0.99	213.73	0.60	0.94	0.40	11.01	0.79

$$\frac{c_e}{q_e} = \frac{1}{q_m K_L} + \frac{c_e}{q_m} \quad (7)$$

$$\ln q_e = \frac{1}{n}\ln c_e + \ln K_F \quad (8)$$

$$\ln\left(\frac{q_e}{q_m - q_e}\right) = \frac{1}{n_s}\ln c_e + \frac{1}{n_s}\ln b \quad (9)$$

$$q_e = B \ln A + B \ln c_e \quad (10)$$

where c_e is the equilibrium concentration (mg L^{-1}), q_e is the amount of heavy metal ion adsorbed at equilibrium (mg g^{-1}), q_m is the maximum metal ion uptake capacity (mg g^{-1}), K_L is the Langmuir constant related to the adsorption energy (L mg^{-1}), $1/n$ is a numerical value related to the adsorption intensity which varies with the heterogeneity, K_F indicates the adsorption capacity, A is the equilibrium constant of binding corresponding to the maximum energy of binding (mg L^{-1}) and the constant B is related to the heat of adsorption (L mg^{-1}). Foe Sips model q_m is the total number of binding sites (mg g^{-1}), b is a Sips constant related to the energy of adsorption (L mg^{-1}) and n_s is the heterogeneity factor. If the parameter n_s is unity, the Langmuir equation is applicable for ideal surfaces. Hence, the parameter n could be regarded as the parameter characterizing system heterogeneity. System heterogeneity could generate from the adsorbent or the adsorbate or a combination of both. The parameter n is usually greater than unity, and larger value for this parameter indicates a more heterogeneous system.

The linear plots for Langmuir, Freundlich, Sips and Temkin are shown in Fig. 15–18. For Langmuir model, the adsorption parameters were calculated from the slope and intercept of a linear plot between c_e/q_e and c_e. Similarly, a plot between $\ln q_e$ vs. $\ln c_e$, $\ln (q_e/q_m - q_e)$ vs. $\ln c_e$ and q_e vs. $\ln c_e$ gives the adsorption parameters for Freundlich, Sips and Temkin model.

The results for each model are presented in Table 2. The determination coefficients, R^2, were used to compare the four isotherm models. As can be seen from Table 2, the Freundlich model showed a higher determination coefficient 0.998 for Pb(II) and 0.995 for Cu(II) than the Langmuir, Sips and Temkin models. The Langmuir–Freundlich (Sips) model revealed, through n values, that the system composed of adsorbent-Pb was less heterogeneous than adsorbent-Cu as larger value of n tends to more heterogeneous surface. Furthermore, the n values from the Sips model also suggested that the Freundlich model can describe the adsorption of Pb(II) and Cu(II) very well. The q_{max} for

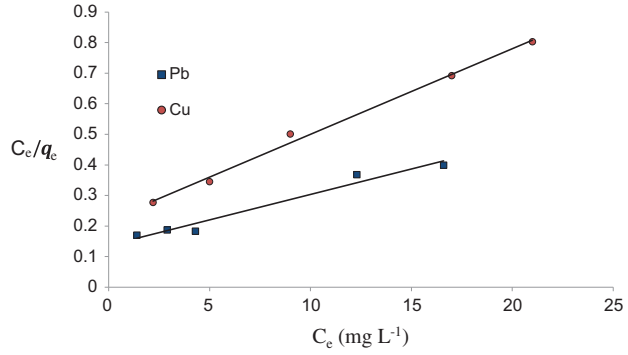

Fig. 15. Langmuir isotherm for Pb(II) and Cu(II) ions at 50°C and pH 5 with 0.05 g adsorbent dosage and pH 5.

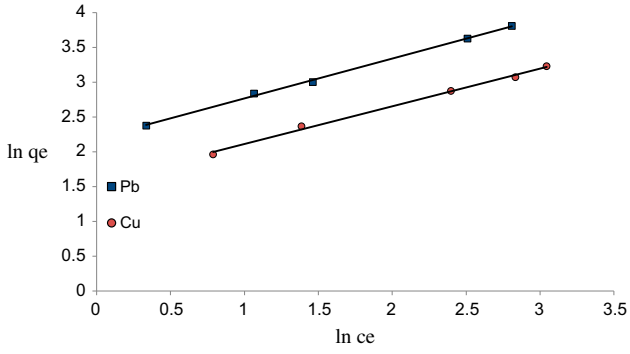

Fig. 16. Freundlich isotherm for Pb(II) and Cu(II) ions at 50°C and pH 5 with 0.05 g adsorbent dosage at pH 5.

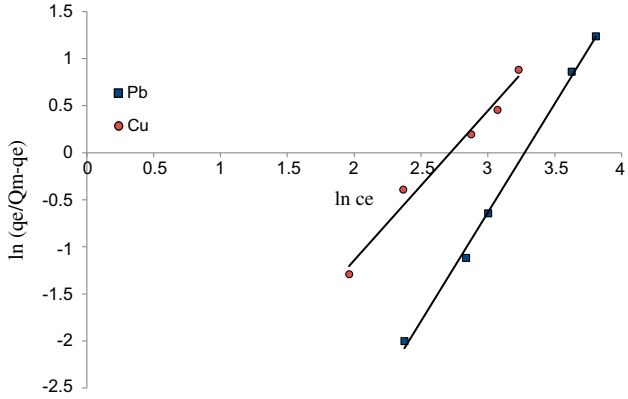

Fig. 17. Sips isotherm for Pb(II) and Cu(II) ions at 50°C and pH 5 with 0.05 g adsorbent dosage.

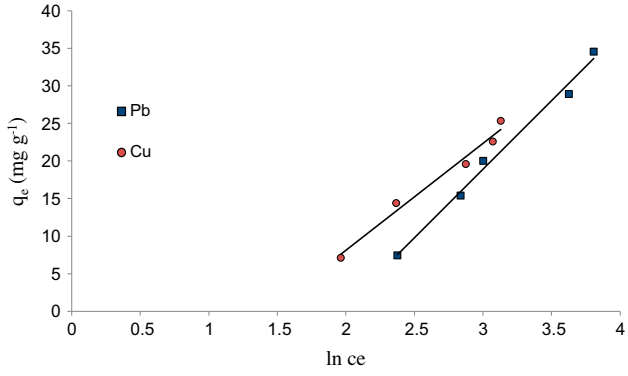

Fig. 18. Temkin isotherm for Pb(II) and Cu(II) ions at 50°C and pH 5 with 0.05 g adsorbent dosage.

Pb(II) and Cu(II) of adsorbent using the Langmuir model was found to be 62.5 and 35.7 mg g^{-1}, respectively. Higher value of binding constant (A) 0.24 for Pb(II) attributes to the high affinity of Pb(II) for adsorbent surface as compare to 0.14 for Cu(II). The B values stands for the heat of adsorption and in this study clearly indicates that the adsorption process is chemisorption.

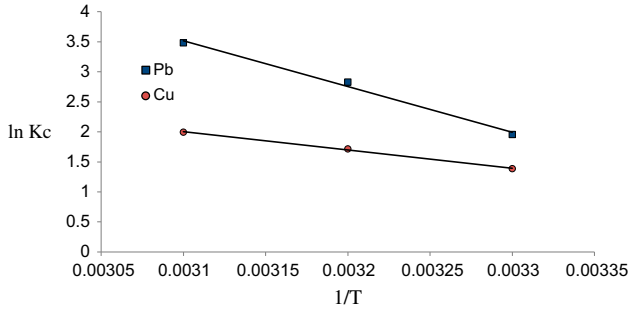

Fig. 19. Thermodynamic plot between ln K_c and $1/T$ at 30, 40 and 50°C.

Table 3
Thermodynamic parameters for Pb(II) and Cu(II) ions adsorption onto Alg-gft-PMMA/Fe_3O_4

Metal ions	ΔH° kJ mol^{-1}	ΔS° J K^{-1} mol^{-1}	ΔG° (kJ mol^{-1})		
			303 K	313 K	323 K
Pb(II)	63.54	225.65	−4.84	−7.09	−9.21
Cu(II)	25.24	94.82	−3.49	−4.44	−5.39

3.5. Thermodynamic studies

To substantiate our prediction about the endothermic nature of the adsorption process, thermodynamic parameters such as Gibbs free energy change (ΔG°), enthalpy change (ΔH°) and entropy change (ΔS°) were calculated using the Gibbs equation and the Van't Hoff equation, listed as follows:

$$\Delta G^\circ = -RT \ln K_c \quad (11)$$

$$\ln K_c = -\frac{\Delta H^\circ}{R} + \frac{\Delta S^\circ}{RT} \quad (12)$$

The gas constant R is defined by 8.3145 J mol^{-1} K^{-1}. K_c (c_{ad}/c_e) is the distribution coefficient; T is the temperature of the solution in Kelvin. ΔG° and ΔS° were

Table 2
Adsorption isotherm parameters of Pb(II) and Cu(II) ions at 50°C

Ions	Langmuir			Freundlich			Sips			Temkin		
	q_m	K_L	R^2	n	K_F	R^2	n_s	b	R^2	A	B	R^2
Pb(II)	62.50	0.12	0.97	1.75	8.94	0.99	0.432	0.04	0.99	0.24	18.23	0.99
Cu(II)	35.71	0.14	0.98	1.85	4.80	0.99	0.630	0.07	0.98	0.14	14.26	0.98

Notes: q_m (mg g^{-1}), K_L (L mg^{-1}), K_F [mg g^{-1}(L/mg)$^{1/n}$], b (L mg^{-1}), A (L g^{-1}), B (J mol^{-1}).

Table 4
Comparison of adsorption capacities (mg g^{-1}) of various adsorbents

Adsorbent	Pb(II)	Cu(II)	Refs.
PMMA/PEI core–shell	–	14.00	[47]
Electrospun Fe_2O_3–Al_2O_3	23.75	4.98	[48]
SMA-EthDA	3.33	100	[49]
Fe_3O_4@TSTC[4]AS-s-SA	19.96	18.11	[50]
PMDA/TMSPEDA	49.72	–	[51]
Sesbania gum-based magnetic carbonaceous	22.7	27.6	[52]
Iron oxide-coated eggshell	–	44.83	[53]
PMMA-gft-Alg/Fe_3O_4	62.50	35.71	This study

calculated from the slop and intercept of a plot of ln K_c as a function of $1/T$, as shown in Fig. 19. The free energy change (ΔG°) can be determined from the following equation:

$$\Delta G^\circ = \Delta H^\circ - T\Delta S^\circ \quad (13)$$

Thermodynamic parameters associated with the Pb(II) and Cu(II) adsorption by the nanocomposite are listed in Table 3. The positive value of ΔH° 63.54 kJ mol^{-1} for Pb(II) and 25.24 kJ mol^{-1} for Cu(II) confirmed the endothermic nature of the adsorption process of Pb(II) and Cu(II). The values of ΔG° are all negative, and the negative value of ΔG° increases as the temperature increases from 30 to 50°C, which indicates that the Pb (II) and Cu(II) adsorption process of the nanocomposite is spontaneous and spontaneity increases with temperature [46]. The positive value of ΔS° 225.65 J mol^{-1} K^{-1} for Pb(II) and 94.82 J mol^{-1} K^{-1} for Cu(II) revealed the increased randomness and an increase in the degrees of freedom at the adsorbent-solution interface during the immobilization of the heavy metal ions on the active sites of the adsorbent, which indicate the partial liberation of the salvation metal ions from solvent molecules before adsorption (liberation of water molecules from solvated-heavy metals), therefore, enabling commonness of randomness and spontaneity in the system.

3.6. Desorption studies

The adsorbed Pb(II) and Cu(II) metal ions could be desorbed by HCl solution (0.1 M, 20 mL) at 30°C. Desorption of Pb(II) and Cu(II) was found to be 87.54 and 89.25%, respectively. The corresponding products after desorption were dried and reused. It was found that the maximum capacities of Pb(II) and Cu(II) were found to be 15.72 and 12.39 mg g^{-1}, respectively, after single desorption. Thus, PMMA-gft-Alg/Fe_3O_4 nanocomposite has great renewable performances and can be used for the adsorption of metal ions.

3.7. Comparison of adsorption capacities

Table 4 presents the comparison of adsorption capacities of various adsorbents with our adsorbent and we found that the adsorbent exhibits very good adsorption capacity towards Pb(II) and Cu(II). Therefore, the present adsorbent can be utilized for successful removal of these metal ions from industrial waste water.

4. Conclusions

The synthesized PMMA-gft-Alg/Fe_3O_4 nanocomposite exhibits excellent capacity for the adsorption of Pb(II) and Cu(II) from aqueous solution. The adsorption of Pb(II) and Cu(II) is highly pH dependent and the maximum adsorption was obtained at pH 5 for both the metal ions. The experimental data were tested using Langmuir, Freundlich, Sips and Temkin models, and the data were best followed by Freundlich model. The kinetic adsorption process can be well described by pseudo-second-order model for the adsorbent. The positive values of ΔH° and ΔS° indicate the adsorption process to be endothermic and spontaneous in nature. Desorption of Pb(II) and Cu(II) was found to be 87.54 and 89.25% in 0.1 M HCl solution, respectively.

Acknowledgements

The authors gratefully acknowledge the instrumentation laboratory, centre for excellence in nanomaterials, Department of Applied Physics, AMU, Sophisticated Analytical Instrumentation Facility (SAIF), Punjab University, Chandigarh, and highly thankful to UGC-MANF New Delhi, for providing financial assistance.

References

[1] Md.R. Awual, Md.M. Hasan, Mu. Naushad, H. Shiwaku, T. Yaita, Preparation of new class composite adsorbent for enhanced palladium(II) detection and recovery, Sens. Actuators, B: Chem. 209 (2015) 790–797.

[2] A. Hanif, H.N. Bhatti, M.A. Hanif, Removal of zirconium from aqueous solution by *Ganoderma lucidum*: Biosorption and bioremediation studies, Desalin. Water Treat. 53 (2015) 195–205.

[3] S.H. Jang, B.G. Min, Y.G. Jeong, W.S. Lyoo, S.C. Lee, Removal of lead ions in aqueous solution by hydroxyapatite/polyurethane composite foams, J. Hazard. Mater. 152 (2008) 1285–1292.

[4] J. Ni, L. Xiong, C. Chen, Q. Chen, Adsorption of Pb(II) and Cd(II) from aqueous solutions using titanate nanotubes prepared via hydrothermal method, J. Hazard. Mater. 189 (2011) 741–748.

[5] A. Selatnia, A. Boukazoula, N. Kechid, M.Z. Bakhti, A. Chergui, Y. Kerchich, Biosorption of lead(II) from aqueous solution by a bacterial dead Streptomyces rimosus biomass, Biochem. Eng. J. 19 (2004) 127–135.

[6] F. Shah, T.G. Kazi, H.I. Afridi, S. Khan, N.F. Kolachi, M.B. Arain, J.A. Baig, The influence of environmental exposure on lead concentrations in scalp hair of children in Pakistan, Ecotoxicol. Environ. Saf. 74 (2011) 727–732.

[7] A. Shahat, Md.R. Awual, Md.A. Khaleque, Md.Z. Alam, Mu. Naushad, A.M.S. Chowdhury, Large-pore diameter nano-adsorbent and its application for rapid lead(II) detection and removal from aqueous media, Chem. Eng. J. 273 (2015) 286–295.

[8] Md.R. Awual, G.E. Eldesoky, T. Yaita, Mu. Naushad, H. Shiwaku, Z.A. AlOthman, S. Suzuki, Schiff based ligand containing nano-composite adsorbent for optical copper(II) ions removal from aqueous solutions, Chem. Eng. J. 279 (2015) 639–647.

[9] N. Li, R. Bai, Copper adsorption on chitosan-cellulose hydrogel beads: Behaviours and mechanisms, J. Appl. Polym. Sci. 42 (2005) 237–245.

[10] M.S. Rahman, M.R. Islam, Effects of pH on isotherms modeling for Cu(II) ions adsorption using maple wood sawdust, Chem. Eng. J. 149 (2009) 273–280.

[11] M. Sener, D.H.K. Reddy, B. Kayan, Bio-sorption properties of pre-treated sporopollen in biomass for lead (II) and copper(II): Application of response surface methodology, Ecol. Eng. 68 (2014) 200–208.

[12] M.A. Hanif, H.N. Bhatti, Remediation of heavy metals using easily cultivable, fast growing and highly accumulating white rot fungi from hazardous aqueous streams, Desalin. Water Treat. 53 (2015) 238–248.

[13] N.V. Suc, H.T.Y. Ly, Lead(II) removal from aqueous solution by chitosan flake modified with citric acid via crosslinking with glutaraldehyde, J. Chem. Technol. Biotechnol. 88 (2013) 1641–1649.

[14] M. Hua, S. Zhang, B. Pan, W. Zhang, L. Lv, Q. Zhang, Heavy metal removal from water/wastewater by nanosized metal oxides: A review, J. Hazard. Mater. 211–212 (2012) 317–331.

[15] A. Shahat, Md.R. Awual, Mu. Naushad, Functional ligand anchored nanomaterial based facial adsorbent for cobalt(II) detection and removal from water samples, Chem. Eng. J. 271 (2015) 155–163.

[16] H.N. Bhatti, S. Hamid, Removal of uranium(VI) from aqueous solutions using *Eucalyptus citriodora* distillation sludge, Int. J. Environ. Sci. Technol. 11 (2014) 813–822.

[17] M. Gorgievski, D. Božić, V. Stanković, N. Štrbac, S. Šerbula, Kinetics, equilibrium and mechanism of Cu^{2+}, Ni^{2+} and Zn^{2+} ions biosorption using wheat straw, Ecol. Eng. 58 (2013) 113–122.

[18] Y. Zhang, L. Yan, W. Xu, X. Guo, L. Cui, L. Gao, Q. Wei, B. Du, Adsorption of Pb(II) and Hg(II) from aqueous solution using magnetic CoFe2O4-reduced graphene oxide, J. Mol. Liq. 191 (2014) 177–182.

[19] J.L. Hu, Q.H. Yang, H. Lin, Y.P. Ye, Q. He, J.N. Zhang, Mesoporous silica nanospheres decorated with CdS nanocrystals for enhanced photocatalytic and excellent antibacterial activities, Nanoscale 5 (2013) 6327–6332.

[20] X.B. Zhang, H.W. Tong, S.M. Liu, G.P. Yong, Y.F. Guan, An improved Stöber method towards uniform and monodisperse Fe_3O_4@C nanospheres, J. Mater. Chem. A 1 (2013) 7488–7493.

[21] K. Semiha, B.U. Omer, K. Erdener, Swelling and dye sorption studies of acrylamide/2-acrylamido-2-methyl-1-propanesulfonic acid/ bentonite highly swollen composite hydrogels, React. Funct. Polym. 68 (2008) 458–473.

[22] D. Hacer, Preparation and characterization of calcium alginate-based composite adsorbents for the removal of Cd, Hg, and Pb ions from aqueous solution, Toxicol. Environ. Chem. 95 (2012) 482–499.

[23] A. Pandey, D. Bera, A. Shukla, L. Ray, Studies on Cr(VI), Pb(II) and Cu(II) adsorption–desorption using calcium alginate as biopolymer, Chem. Sep. Bioavailability 19 (2007) 17–24.

[24] K. Rathinam, M. Sankaran, Removal of Cr(VI) ions by adsorption onto sodium alginate-polyaniline nanofibers, J. Biol. Macromol. 72 (2015) 711–717.

[25] A.I. Zouboulis, I.A. Katsoyiannis, Arsenic removal using iron oxide loaded alginate beads, Ind. Eng. Chem. Res. 41 (2002) 6149–6155.

[26] K. Tae-Youb, Y. Yohtaro, H. Teruyoshi, Magneto-optical properties of Bi-YIG nanoparticle with polymethacrylate matrix materials, Phys. Status Solidi B 241 (2004) 1601–1604.

[27] Q. Lei, H. Xi-Wen, L. Wen-You, Z. Yu-Kui, Molecularly imprinted polymer prepared with bonded β-cyclodextrin and acrylamide on functionalized silica gel for selective recognition of tryptophan in aqueous media, J. Chromatogr. A 1187 (2008) 94–102.

[28] Q. Li, M.H.W. Lam, R.S.S. Wu, B. Jiang, Rapid magnetic-mediated solid-phase extraction and pre-concentration of selected endocrine disrupting chemicals in natural waters by poly(divinylbenzene-co-methacrylic acid) coated Fe_3O_4 core–shell magnetite microspheres for their liquid chromatography–tandem mass spectrometry determination, J. Chromatogr. A 1217 (2010) 1219–1226.

[29] Y.H. Zheng, Y. Cheng, F. Bao, Y.S. Wang, Synthesis and magnetic properties of Fe_3O_4 nanoparticles, Mater. Res. Bull. 41 (2006) 525–529.

[30] T.A. Sreenivasan, R. Sreenivasan, A.R. Tharun, Adsorptive removal of thorium(IV) from aqueous solutions using poly (methacrylic acid)-grafted chitosan/bentonite composite matrix: Process design and equilibrium studies, Colloids Surf. A: Physicochem. Eng. Aspects 368 (2010) 13–22.

[31] Z.P. Yang, X.Y. Gong, C.J. Zhang, Recyclable Fe_3O_4/hydroxyapatite composite nanoparticles for photocatalytic applications, Chem. Eng. J. 165 (2010) 117–121.
[32] Y. Vijaya, S.R. Popuri, V.M. Boddu, A. Krishnaiah, Modified chitosan and calcium alginate biopolymer sorbents for removal of nickel(II) through adsorption, Carbohydr. Polym. 72 (2008) 261–271.
[33] G. Duan, C. Zhang, A. Li, X. Yang, L. Lu, X. Wang, Preparation and characterization of mesoporous zirconia made by using a poly (methyl methacrylate) template, Nanoscale Res. Lett. 3 (2008) 118–122.
[34] S. Sadeghi, H. Azhdari, H. Arabi, A.Z. Moghaddam, Surface modified magnetic Fe_3O_4 nanoparticles as a selective sorbent for solid phase extraction of uranyl ions from water samples, J. Hazard. Mater. 215–216 (2012) 208–216.
[35] E. Kandare, H. Deng, D. Wang, J.M. Hossenlopp, Thermal stability and degradation kinetics of poly (methyl methacrylate)/layered copper hydroxy methacrylate composites, Polym. Adv. Technol. 17 (2006) 312–319.
[36] T.S. Anirudhan, A.R. Tharun, S.R. Rejeena, Investigation on poly(methacrylic acid)-grafted cellulose/bentonite superabsorbent composite: Synthesis, characterization, and adsorption characteristics of bovine serum albumin, Ind. Eng. Chem. Res. 50 (2011) 1866–1874.
[37] H. Hasar, Adsorption of nickel(II) from aqueous solution onto activated carbon prepared from almond husk, J. Hazard. Mater. 97 (2003) 49–57.
[38] M. Arshadi, F. Salimi Vahid, J.W.L. Salvacion, M. Soleymanzadeh, A practical organometallic decorated nano-size SiO-Al_2O_3 mixed-oxides for methyl orange removal from aqueous solution, Appl. Surf. Sci. 280 (2013) 726–736.
[39] A.E. Ofomaja, E.B. Naidoo, S.J. Modise, Kinetic and pseudo-second-order modeling of lead biosorption onto pine cone powder, Ind. Eng. Chem. Res. 49 (2010) 2562–2572.
[40] G. Zhang, Z. Ren, X. Zhang, J. Chen, Nanostructured iron(III)-copper(II) binary oxide: A novel adsorbent for enhanced arsenic removal from aqueous solutions, Water Res. 47 (2013) 4022–4031.
[41] K.G. Bhattacharyya, A. Sharma, *Azadirachta indica* leaf powder as an effective biosorbent for dyes: A case study with aqueous Congo Red solutions, J. Environ. Manage. 71 (2004) 217–229.
[42] R. Qu, Y. Zhang, C. Sun, C. Wang, C. Ji, H. Chen, P. Yin, Adsorption of Hg(II) from an aqueous solution by silica-gel supported diethylenetriamine prepared via different routes: Kinetics, thermodynamics, and isotherms, J. Chem. Eng. Data 55 (2010) 1496–1504.
[43] H. Wang, X. Yuan, Y. Wu, H. Huang, G. Zeng, Y. Liu, X. Wang, N. Lin, Y. Qi, Adsorption characteristics and behaviors of graphene oxide for Zn(II) removal from aqueous solution, Appl. Surf. Sci. 279 (2013) 432–440.
[44] E. Repo, J.K. Warchol, T.A. Kurniawan, M.E.T. Sillanpää, Adsorption of Co(II) and Ni(II) by EDTA- and/or DTPA-modified chitosan: Kinetic and equilibrium modeling, Chem. Eng. J. 161 (2010) 73–82.
[45] X. Wang, A. Wang, Removal of Cd(II) from aqueous solution by a composite hydrogel based on attapulgite, Environ. Technol. 31 (2010) 745–753.
[46] A. Sari, D. Mendil, M. Tuzen, M. Soylak, Biosorption of palladium(II) from aqueous solution by moss (*Racomitrium lanuginosum*) biomass: Equilibrium, kinetic and thermodynamic studies, J. Hazard. Mater. 162 (2009) 874–879.
[47] A. Wu, J. Jia, S. Luan, Amphiphilic PMMA/PEI core–shell nanoparticles as polymeric adsorbents to remove heavy metal pollutants. Colloids Surf., A: Physicochem. Eng. Aspects 384 (2011) 180–185.
[48] A. Mahapatra, B.G. Mishra, G. Hota, Electrospun Fe_2O_3-Al_2O_3 nanocomposite fibers as efficient adsorbent for removal of heavy metal ions from aqueous solution, J. Hazard. Mater. 258–259 (2013) 116–123.
[49] E. Abo-Baker, S.S. Elkholy1, M.Z. Elsabee, Modified poly (styrene maleic anhydride) copolymer for the removal of toxic metal cations from aqueous solutions, Am. J. Polym. Sci. 5 (2015) 55–64.
[50] M.M. Lakouraj, F. Mojerlou, E.N. Zare, Nanogel and superparamagnetic nanocomposite based on sodium alginate for sorption of heavy metal ions, Carbohydr. Polym. 106 (2014) 34–41.
[51] I.H. Alsohaimi, S.M. Wabaidur, M. Kumar, M.A. Khan, Z.A. Alothman, M.A. Abdalla, Synthesis, characterization of PMDA/TMSPEDA hybrid nanocomposite and its applications as an adsorbent for the removal of bivalent heavy metals ions, Chem. Eng. J. 270 (2015) 9–21.
[52] S. Lan, Z. Leng, N. Guo, X. Wu, S. Gan, Sesbania gum-based magnetic carbonaceous nanocomposites: Facile fabrication and adsorption behavior, Colloids Surf., A: Physicochem. Eng. Aspects 446 (2014) 163–171.
[53] R. Ahmad, R. Kumar, S. Haseeb, Adsorption of Cu^{2+} from aqueous solution onto iron oxide coated eggshell powder: Evaluation of equilibrium, isotherms, kinetics, and regeneration capacity, Arab. J. Chem. 5 (2012) 353–359.